Enhanced and tunable Imbert–Fedorov shift based on epsilon-near-zero response of Weyl semimetal

Ji-Peng Wu(伍计鹏)[1,2], Yuan-Jiang Xiang(项元江)[2], and Xiao-Yu Dai(戴小玉)[2,†]

[1] *College of Railway Transportation, Hunan University of Technology, Zhuzhou* 412007, *China*
[2] *College of Electrical and Information Engineering, Hunan University, Changsha* 410082, *China*

(Received 14 May 2022; revised manuscript received 5 July 2022; accepted manuscript online 8 July 2022)

We theoretically investigate the reflected spatial Imbert–Fedorov (IF) shift of transverse-electric (TE)-polarized beam illuminating on a bulk Weyl semimetal (WSM). The spatial IF shift is enhanced significantly at two different frequencies close to the epsilon-near-zero (ENZ) frequency, where large values of reflection coefficients $|r_{pp}|/|r_{ss}|$ are obtained due to the ENZ response induced different rapid increasing trends of $|r_{pp}|$ and $|r_{ss}|$. Particularly, the tunable ENZ effect with tilt degree of Weyl cones and Fermi energy enables the enhanced spatial IF shift at different frequencies. The enhanced spatial IF shift also shows the adjustability of WSM thickness, incident angle and Weyl node separation. Our findings provide easy and available methods to enlarge and adjust the reflected IF shift of TE-polarized light with a WSM.

Keywords: Imbert–Fedorov shift, Weyl semimetal, epsilon-near-zero, reflection

PACS: 75.70.Tj, 78.20.Ci **DOI:** 10.1088/1674-1056/ac7f92

1. Introduction

For a bound light beam, the geometrical optics is usually not sufficient to accurately represent the reflection characteristics.[1] The reflected light generates a shift in a direction perpendicular to the incident plane, which is named Imbert–Fedorov (IF) shift.[1,2] The IF shift is spin-dependent and also named spin Hall effect of light, since it emerges because of the spin–orbit interaction, and follows the conservation law of angular momentum.[2,3] Generally, the IF shift is tiny with its value on the subwavelength scale, so conventional experimental methods are not capable of measuring the value directly.[1,4] Recently, the enhancement of the IF shift has attracted profound interests due to its applications in optical devices, such as detectors,[5] sensors,[6] *etc*. It has been proved that the enhanced IF shift of the reflected light can be realized by restricting the co-polarized reflection coefficients.[7–11] Notably, Brewster effect and plasmon act as most commonly methods to restrain the co-polarized reflection coefficients.[8–11] However, the Brewster angle often exists in the situation of the transverse-magnetic (TM)-polarized incident wave, while it may not exist in the transverse-electric (TE)-polarized incident light, so the enhanced IF shift is usually realized in the TM-polarized beam. Additionally, although plasmon denotes the effective method to achieve the suppressed reflection coefficients of TM- and TE-polarized waves, the excitation of plasmon should solve the condition of wave vector mismatch.

Weyl semimetal (WSM), denoting a striking topological material which takes the nonmass Weyl fermions as the quasi-particles, emerges only by breaking the symmetry of spatial or time inversion.[12] WSM denotes a graphene analogous Dirac-like linear dispersion, which generates numerous excellent optical performances, such as controlled plasmon resonance[13] and distinctive optical nonlinearity.[14] Notably, WSM represents a three-dimensional Hamiltonian different from the two-dimensional graphene, which reveals numerous unique physical features, such as remarkable quantum Hall effect,[8,9] chiral anomalies,[15,16] *etc*. Furthermore, the Weyl nodes of WSM play as a sink or source of the Berry curvature, serving as the equivalent magnetic field in momentum space,[17,18] so the optical responses of WSMs should be represented with the axion electrodynamics.[19,20] Meanwhile, the off-diagonal components of the dielectric constant tensor emerge because of the magnetic field, resulting in the existence of the cross-polarized reflection and transmission coefficients.[21] Recently, numerous optical phenomena in WSM based systems have been discussed, such as adjustable Goos–Hänchen shift,[22,23] large Kerr and Faraday effects,[21,24] anomalous Hall effects,[25–27] *etc*. Nevertheless, to our knowledge, these works about the enhanced reflected IF shift mainly restrict the co-polarized reflection coefficient $|r_{pp}|$ by exciting the Brewster effect. Therefore, the feasible enhanced reflected IF shifts of the TE-polarized incident beam in Weyl based systems with other easy and available methods exhibit fatal research significance.

Epsilon-near-zero (ENZ) material, on the other side, acting as a new type of material, presenting near-zero or zero permittivity at one or multiple frequencies, has received broad interests in photonics.[28–30] Notably, tunable ENZ response has been discovered in WSM.[31] Therefore, WSM with tun-

†Corresponding author. E-mail: xiaoyudai@126.com

© 2023 Chinese Physical Society and IOP Publishing Ltd

able ENZ effect supplies a significant research channel to discuss the adjustable enhanced reflected spatial IF shifts of the TE-polarized beam. In this paper, we theoretically investigate the reflected spatial IF shift induced by the TE-polarized light illuminating on a bulk WSM at the frequencies close to the ENZ frequency. The enhanced spatial IF shift can be enlarged by decreasing the Weyl node separation. Our findings provide easy and available methods to enlarge and adjust the reflected IF shift of the TE-polarized wave with a WSM.

2. Theoretical model and method

To investigate the spatial IF shift of the reflected light in WSM based system, a simple structure is proposed as Fig. 1(a). Our schematic contains three regions, denoted as air 0, bulk WSM 1, and air 2. For the line polarized light impinging at the surface of the WSM with incident angle θ, reflection appears at the interface of air 0 and WSM, thus lead to the relevant spatial IF shift, denoted as Δ. Figure 1(b) exhibits the type-I ($\beta < 1$) WSMs, where the parameters $\beta = \beta_s$, $s = \pm$ represent the tilt degree of Weyl cones that distinguish the diversity of type-I and type-II phases.[31] For the type-I WSM, the parameters β_s meet $\beta_s < 1$, while β_s meet $\beta_s > 1$ for the type-II WSM.

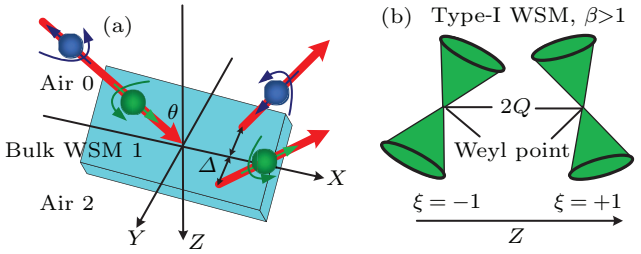


Fig. 1. Schematic representing the spatial IF shift. Panel (a) denotes a line polarized beam illuminating on the bulk WSM with thickness of d, and the spatial IF shift of the reflected beam occurs. Panel (b) represents two Weyl cones with contrary chirality in the type-I WSM, in which Q exhibits the Weyl node separation toward the z direction.

Generally, the mode dispersion diagram of WSM shows the temperature, impurities, and disorder dependence, so the temperature is treated as zero, and the influences of impurities and disorder are overlooked for clarity. A system composed of two Weyl cones, named the WSM, appears by breaking time-reversal symmetry. Through stacking the ferromagnet blocks and topological insulator into multiple thin films, the WSM materials can be obtained.[12] Around the two Weyl cones, the Weyl Hamiltonian at low energy physics can be written as a 2×2 matrix[12,31,32]

$$\boldsymbol{H}_s = v_{\mathrm{F}}\left[\beta_s\left(p_z - sQ\right) + s\boldsymbol{\sigma}\left(\boldsymbol{p} - sQ\boldsymbol{e}_z\right)\right], \tag{1}$$

where $v_{\mathrm{F}} = 10^6$ m/s is the Fermi velocity, $\boldsymbol{\sigma}$ represents the Pauli matrix, $\boldsymbol{p}$ displays the momentum vector, and $\boldsymbol{e}_z$ and p_z denote the unit vector and momentum component in the z direction, respectively.

Particularly, considering the WSM with a separated pair of nodes toward the z axis in Brillouin zone (BZ) in Fig. 1(b), the permittivity tensor ε can be written as[31]

$$\varepsilon = \begin{bmatrix} \varepsilon_{xx} & \varepsilon_{xy} & 0 \\ \varepsilon_{yx} & \varepsilon_{yy} & 0 \\ 0 & 0 & \varepsilon_{zz} \end{bmatrix}, \tag{2}$$

where $\varepsilon_{xx} = \varepsilon_{yy} = \varepsilon_{\parallel}$ represent the interface parallel components, ε_{zz} exhibits the interface perpendicular component, and $\varepsilon_{xy} = -\varepsilon_{yx} = \mathrm{i}\gamma$ denote the off-diagonal components. All components depend on the angular frequency ω, in which ε_{xx} can be written as[31]

$$\varepsilon_{xx}(\omega) = 1 + \frac{\alpha}{3\pi}\left[\ln\left|\frac{4\Gamma^2}{4\mu^2-\omega^2}\right| - \frac{4\mu^2}{\omega^2} + \mathrm{i}\pi\Theta(\omega - 2\mu)\right], \tag{3}$$

where $\alpha = e^2/(4\pi\varepsilon_0\hbar v_{\mathrm{F}})$ represents the fine structure constant, μ denotes the Fermi energy, ε_0 displays the permittivity in vacuum, $\hbar$ represents the reduced Planck constant, e exhibits the charge of electron, $\Gamma = 8v_{\mathrm{F}}|Q|$ denotes the energy cut-off, and $\Theta(X)$ is the usual step function. Meanwhile, the components ε_{zz} and γ not only denote as a function of ω, but also exhibit the dependence of β_s. For the type-I WSM, ε_{zz} and γ are approximately written as[31]

$$\begin{aligned}
\varepsilon'_{zz} = {} & 1 + \frac{\alpha\mu^2}{\pi\omega^2}\sum_{s=\pm}\frac{1}{\beta_s^3}\left\{\frac{8}{3}\beta_s - 4\arctan h\beta_s\right. \\
& + \ln\left|\frac{4\mu^2-\omega^2(1+\beta_s)^2}{4\mu^2-\omega^2(1-\beta_s)^2}\right| \\
& + \frac{\omega^2}{12\mu^2}\sum_{t=\pm 1}\left[t(1+2t\beta_s)(1-t\beta_s)^2\right. \\
& \times \ln\left|\frac{4\Gamma^2(1-t\beta_s)^2}{4\mu^2-\omega^2(1-t\beta_s)^2}\right| \\
& - \frac{2\mu}{\omega}\left(\frac{4\mu^2}{\omega^2} + 3 - 3\beta_s^2\right) \\
& \left.\left.\times \ln\left|\frac{2\mu - t\omega(1+t\beta_s)}{2\mu + t\omega(1+t\beta_s)}\right|\right]\right\},
\end{aligned} \tag{4}$$

$$\begin{aligned}
\varepsilon''_{zz} = {} & \frac{\alpha}{6}\sum_{s=\pm}\Theta\left(\omega - \frac{2\mu}{1+|\beta_s|}\right)\left(1 - \frac{1}{2}\left\{1 + \frac{3}{2|\beta_s|}\left(\frac{2\mu}{\omega} - 1\right)\right.\right. \\
& \left.\left.\times\left[1 - \frac{1}{3\beta_s^2}\left(\frac{2\mu}{\omega} - 1\right)^2\right]\right\}\Theta\left(\frac{2\mu}{1-|\beta_s|} - \omega\right)\right),
\end{aligned} \tag{5}$$

$$\gamma = \frac{\alpha}{\pi\omega}\left[2v_{\mathrm{F}}Q - \sum_{s=\pm}\frac{s\mu}{2\beta_s}\left(\frac{1}{\beta_s}\ln\left|\frac{1+\beta_s}{1-\beta_s}\right| - 2\right)\right], \tag{6}$$

where ε'_{zz} and ε''_{zz} exhibit the real and imaginary components of ε_{zz}.

In our proposed structure, there has no Fermi arc state at x–y plane because of a separated pair of nodes toward the z axis in BZ. Therefore, the tangential magnetic and electric fields maintain continuity at $z = 0$ and d surfaces.[21] Nevertheless, because of the separated polarization of electromagnetic beams in WSM,[9,31] the reflection coefficients cannot be solved by using the 2×2 transfer matrix method, and a 4×4 magneto–optical matrix is utilized to settle the situation.[9]

Generally, for a monochromatic Gaussian beam with finite beam width illuminating on the WSM, the angular spectrum can be described as

$$\boldsymbol{E}_{\mathrm{i}}\left(k_{\mathrm{i}x},k_{\mathrm{i}y}\right)=\exp\left[-\frac{w_0^2\left(k_{\mathrm{i}x}^2+k_{\mathrm{i}y}^2\right)}{4}\right]\boldsymbol{f}, \tag{7}$$

where w_0 denotes the beam waist. $k_{\mathrm{i}x}$ and $k_{\mathrm{i}y}$ represent the components of the incident beam vector in the x and y directions, respectively. The polarization of the incident beam is represented by a unit complex vector $\boldsymbol{f}=\left(\boldsymbol{x}_{\mathrm{i}}f_{\mathrm{p}}+\boldsymbol{y}_{\mathrm{i}}f_{\mathrm{s}}\right)$, in which $f_{\mathrm{s}}=a_{\mathrm{TE}}\exp\left(\mathrm{i}\eta\right)$ and $f_{\mathrm{p}}=a_{\mathrm{TM}}\in R$. Therefore, the reflected polarization state relative to the incident polarization state can be expressed as[8]

$$\begin{bmatrix}\boldsymbol{E}_{\mathrm{p}}^{(\mathrm{r})}\\ \boldsymbol{E}_{\mathrm{s}}^{(\mathrm{r})}\end{bmatrix}=\begin{bmatrix}r_{\mathrm{pp}} & r_{\mathrm{sp}}+\dfrac{k_{\mathrm{r}y}\cot\theta\left(r_{\mathrm{pp}}+r_{\mathrm{ss}}\right)}{k_0}\\ r_{\mathrm{ps}}-\dfrac{k_{\mathrm{r}y}\cot\theta\left(r_{\mathrm{pp}}+r_{\mathrm{ss}}\right)}{k_0} & r_{\mathrm{ss}}\end{bmatrix}\begin{bmatrix}\boldsymbol{E}_{\mathrm{p}}^{(\mathrm{i})}\\ \boldsymbol{E}_{\mathrm{s}}^{(\mathrm{i})}\end{bmatrix}, \tag{8}$$

where $r_{\mathrm{pp}}=E_{\mathrm{r}}^{\mathrm{p}}/E_{\mathrm{i}}^{\mathrm{p}}$, $r_{\mathrm{sp}}=E_{\mathrm{r}}^{\mathrm{p}}/E_{\mathrm{i}}^{\mathrm{s}}$, $r_{\mathrm{ss}}=E_{\mathrm{r}}^{\mathrm{s}}/E_{\mathrm{i}}^{\mathrm{s}}$, $r_{\mathrm{ps}}=E_{\mathrm{r}}^{\mathrm{s}}/E_{\mathrm{i}}^{\mathrm{p}}$ denote the Fresnel reflection coefficients for parallel and perpendicular polarizations. $k_{\mathrm{r}x}$ and $k_{\mathrm{r}y}$ are the components of the reflected beam vector in the x and y directions, respectively. Based on the boundary conditions $k_{\mathrm{r}x}=-k_{\mathrm{i}x}$ and $k_{\mathrm{r}y}=k_{\mathrm{i}y}$, and applying the Taylor series expansion upon reflection, the reflected field can be further denoted as

$$\begin{aligned}\boldsymbol{E}_{\mathrm{r}}=&\exp\left[-\frac{w_0^2\left(k_{\mathrm{r}x}^2+k_{\mathrm{r}y}^2\right)}{4}\right]\\&\times\left\{\boldsymbol{x}_{\mathrm{r}}\left[f_{\mathrm{p}}r_{\mathrm{pp}}+f_{\mathrm{s}}r_{\mathrm{sp}}+\frac{f_{\mathrm{s}}k_{\mathrm{r}y}\left(r_{\mathrm{pp}}+r_{\mathrm{ss}}\right)\cot\theta}{k_0}\right]\right.\\&\left.+\boldsymbol{y}_{\mathrm{r}}\left[f_{\mathrm{s}}r_{\mathrm{ss}}+f_{\mathrm{p}}r_{\mathrm{ps}}-\frac{f_{\mathrm{p}}k_{\mathrm{r}y}\left(r_{\mathrm{pp}}+r_{\mathrm{ss}}\right)\cot\theta}{k_0}\right]\right\}.\end{aligned} \tag{9}$$

Applying paraxial approximation and the Fourier transformation, the complex amplitude of the reflected beam can be denoted as

$$\begin{aligned}\boldsymbol{E}_{\mathrm{r}}\left(x_{\mathrm{r}},y_{\mathrm{r}},z_{\mathrm{r}}\right)=&\iint\mathrm{d}k_{\mathrm{r}x}\mathrm{d}k_{\mathrm{r}y}\boldsymbol{E}_{\mathrm{r}}\left(k_{\mathrm{r}x},k_{\mathrm{r}y}\right)\\&\times\exp\left[\mathrm{i}\left(k_{\mathrm{r}x}x_{\mathrm{r}}+k_{\mathrm{r}y}y_{\mathrm{r}}-\frac{k_{\mathrm{r}x}^2+k_{\mathrm{r}y}^2}{2k_0}\right)\right].\end{aligned} \tag{10}$$

In position space, the general expression of the reflected angular spectrum can be described as

$$\begin{aligned}\boldsymbol{E}_{\mathrm{r}}=&\exp\left(\mathrm{i}kz_{\mathrm{r}}-\frac{k}{2}\frac{x_{\mathrm{r}}^2+y_{\mathrm{r}}^2}{\Lambda_{\mathrm{R}}+\mathrm{i}z_{\mathrm{r}}}\right)\\&\times\left\{\boldsymbol{x}_{\mathrm{r}}\left[f_{\mathrm{p}}r_{\mathrm{pp}}+f_{\mathrm{s}}r_{\mathrm{sp}}+f_{\mathrm{s}}\frac{\mathrm{i}y_{\mathrm{r}}\left(r_{\mathrm{pp}}+r_{\mathrm{ss}}\right)\cot\theta}{\Lambda_{\mathrm{R}}+\mathrm{i}z_{\mathrm{r}}}\right]\right.\\&\left.+\boldsymbol{y}_{\mathrm{r}}\left[f_{\mathrm{s}}r_{\mathrm{ss}}+f_{\mathrm{p}}r_{\mathrm{ps}}-f_{\mathrm{p}}\frac{\mathrm{i}y_{\mathrm{r}}\left(r_{\mathrm{pp}}+r_{\mathrm{ss}}\right)\cot\theta}{\Lambda_{\mathrm{R}}+\mathrm{i}z_{\mathrm{r}}}\right]\right\},\end{aligned} \tag{11}$$

where $\Lambda_{\mathrm{R}}=k_1w_0^2/2$ represents the Rayleigh range.

The IF shift of the beam appears in the directions perpendicular to the plane of the incidence. At any given plane $z_{\mathrm{r}}=\mathrm{const}$, the IF shift of the field centroid can be written as

$$\Delta_{\mathrm{IF}}=\frac{\iint y_{\mathrm{r}}I\left(x_{\mathrm{r}},y_{\mathrm{r}},z_{\mathrm{r}}\right)\mathrm{d}x_{\mathrm{r}}\mathrm{d}y_{\mathrm{r}}}{\int I\left(x_{\mathrm{r}},y_{\mathrm{r}},z_{\mathrm{r}}\right)\mathrm{d}x_{\mathrm{r}}\mathrm{d}y_{\mathrm{r}}}. \tag{12}$$

Here, when the irrelevant proportionality factor is neglected, the intensity is directly proportional to the absolute square of the reflected angular spectrum, *i.e.*, $I\left(x_{\mathrm{r}},y_{\mathrm{r}},z_{\mathrm{r}}\right)\propto\left|E_{\mathrm{R}}\right|^2$. Ultimately, for the TE-polarized light impinging at the surface of the WSM, the reflected light occurs, and the related spatial IF beam shift can be simplified and written as[8]

$$\Delta=\frac{R_{\mathrm{sp}}\cot\theta\left[R_{\mathrm{pp}}\sin\left(\Phi_{\mathrm{sp}}-\Phi_{\mathrm{pp}}\right)+R_{\mathrm{ss}}\sin\left(\Phi_{\mathrm{sp}}-\Phi_{\mathrm{ss}}\right)\right]}{k_0\left(R_{\mathrm{sp}}^2+R_{\mathrm{ss}}^2\right)}. \tag{13}$$

where k_0 is the wave vector of vacuum, R_j and Φ_j denote the amplitude and phase of reflection coefficients r_j, respectively, where $j=\mathrm{pp},\mathrm{ss},\mathrm{sp}$.

3. Results and discussion

The possibility of altering Fermi energy acts as a spectacular feature of WSM. It is successful to control the Fermi energy by changing the charge neutrality point via doping, adjusting the lattice constant via pressure variations, or varying the temperature.[33,34] To illustrate the effects of Fermi energy on the ENZ response, figure 2(a) plots the real part of ε_{zz} at various Fermi energies. The tilt degree and Weyl node separation are set as 0.8 nm^{-1} and 1 nm^{-1}, respectively. Notably, the ENZ effect can be obtained at various Fermi energies of $0.39v_{\mathrm{F}}|Q|$, $0.4v_{\mathrm{F}}|Q|$, $0.41v_{\mathrm{F}}|Q|$, and $0.42v_{\mathrm{F}}|Q|$. The relevant ENZ frequency rises with the increase of Fermi energy. Particularly, the ENZ response occurs at 50.87 THz, 52.3 THz, 53.73 THz, and 55.17 THz for Fermi energy of $0.39v_{\mathrm{F}}|Q|$, $0.4v_{\mathrm{F}}|Q|$, $0.41v_{\mathrm{F}}|Q|$, and $0.42v_{\mathrm{F}}|Q|$, respectively. Furthermore, the tilt degree plays as other special and significant parameter for characterizing the optical features of WSM. The real part of ε_{zz} also shows important correlation with the tilt degree. Figure 2(b) denotes the real part of ε_{zz} at various tilt degrees. The Fermi energy and Weyl node separation are chosen as $0.4v_{\mathrm{F}}|Q|$ and 1 nm^{-1}, respectively. It is found that the ENZ effect always exists at various tilt degrees of 0.78, 0.8, 0.82, and 0.84. The relevant ENZ frequency increases from 51.22 THz to 54.88 THz as the tilt degree rises from 0.78 to

0.84. Therefore, the adjustable ENZ effects are obtained with tilt degree and Fermi energy, thus lead to the feasible adjustability of the enhanced spatial IF shift.

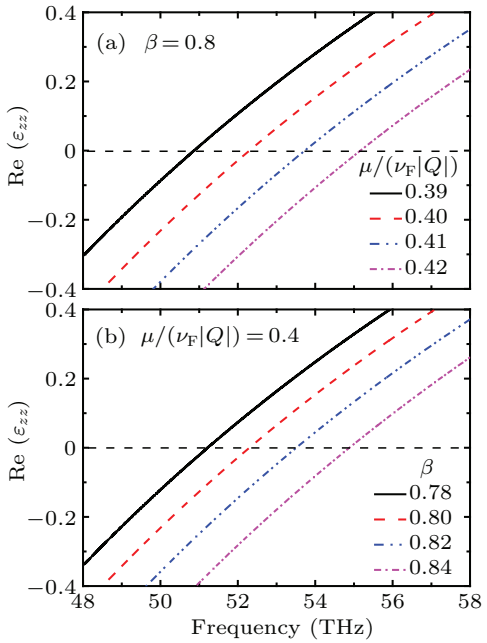


Fig. 2. The adjustable ENZ response. Panels (a) and (b) exhibit the real part of ε_{zz} as a function of frequency by altering the Fermi energy and tilt degree.

As known from the calculated expression of the spatial IF shift, it can be enhanced significantly when the reflection coefficient $|r_{ss}|$ is acquired to a smaller value relative to the reflection coefficients $|r_{pp}|$ and $|r_{sp}|$. Generally, $|r_{ss}|$ has a larger value than $|r_{sp}|$, and is close to the value of $|r_{pp}|$. Therefore, for the reflected spatial IF shift of the TE-polarized light, it is difficult to achieve a large enhancement. To demonstrate the feasibility of the enhanced spatial IF shift in our structure, figure 3(a) shows the spatial IF shift as a function of frequency. The thickness d is selected as 60 nm, and the incident angle θ is set as 20°. It is worth noting that the absolute spatial IF shift retains a relatively large value at the frequencies away from the ENZ frequency. More importantly, as the frequency increases to the ENZ frequency, the curve of the spatial IF shift first declines sharply, and then increase steeply. In other word, the maximal enhanced spatial IF shifts of nearly -11.1 μm at the frequency of 52.26 THz, and of nearly 11.3 μm at the frequency of 52.34 THz are obtained, in which the positive and negative spatial IF shifts are mainly caused by the phase differences of reflection coefficients. To further analyze the causes of the enhanced spatial IF shift in detail, figures. 3(b) and 3(c) denote the amplitude of $|r_{pp}|$, $|r_{ss}|$, and $|r_{sp}|$, and the value of $|r_{pp}|/|r_{ss}|$ and $|r_{sp}|/|r_{ss}|$ as a function of frequency, respectively. Notably, both $|r_{pp}|$ and $|r_{ss}|$ maintain their respective small values at the frequencies away from the ENZ frequency, and rise to their respective maximal values rapidly as the frequency increases to the ENZ frequency. Furthermore, it is must be noticed that the increasing trends of $|r_{pp}|$ and $|r_{ss}|$ at frequencies close to the ENZ frequency behave differently, which provides the feasibility to achieve the enhanced spatial IF shift. It is also seen that the maximal values of $|r_{pp}|/|r_{ss}|$ display differently at two different frequencies close to the ENZ frequency, and are much larger than the values of $|r_{sp}|/|r_{ss}|$. In a word, it is well demonstrated that the large values of $|r_{pp}|/|r_{ss}|$ are obtained at two different frequencies due to the ENZ response induced different rapid increasing trends of $|r_{pp}|$ and $|r_{ss}|$, thus enhance the spatial IF shift significantly.

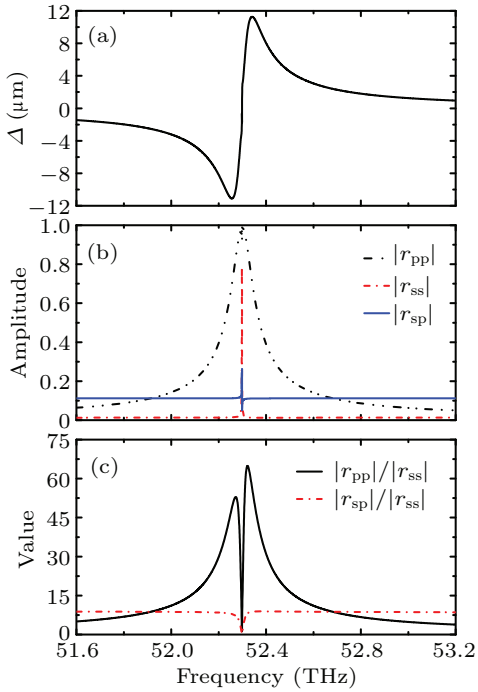


Fig. 3. The enhanced spatial IF shift. Panel (a) plots the spatial IF shift as a function of frequency. Panel (b) shows the amplitude of $|r_{pp}|$, $|r_{ss}|$, and $|r_{sp}|$ as a function of frequency. Panel (c) denotes the value of $|r_{pp}|/|r_{ss}|$ and $|r_{sp}|/|r_{ss}|$ as a function of frequency. Where the Fermi energy and tilt degree are set as $0.4\nu_F|Q|$ and 0.8, respectively. Other parameters are the same of Fig. 2.

Notably, the value of $|r_{pp}|/|r_{ss}|$ is enlarged markedly because of the ENZ effect of WSM, so the spatial IF shift is enhanced significantly. Meanwhile, tilt degree and Fermi energy reveal effective methods to acquire the ENZ effect at different frequencies. Therefore, the large enhanced spatial IF shift can be achieved readily at various frequencies by changing the tilt degree and Fermi energy. The spatial IF shifts at various tilt degrees and Fermi energies are exhibited in Fig. 4. It is found that at various Fermi energies, the enhanced spatial IF shift can always be obtained at two different frequencies close to the corresponding ENZ frequencies. Similarly, the enhancement of the spatial IF shift can be realized at two different frequencies close to the relevant ENZ frequency by altering the tilt degree, as seen in Fig. 4(b). In a word, the tunable ENZ effect with tilt degree and Fermi energy enables the controllable enhanced spatial IF shift. Additionally, the tunable spatial IF

shift varying from negative to positive with tilt degree enables the precise determination of WSM tilt degree.[9]

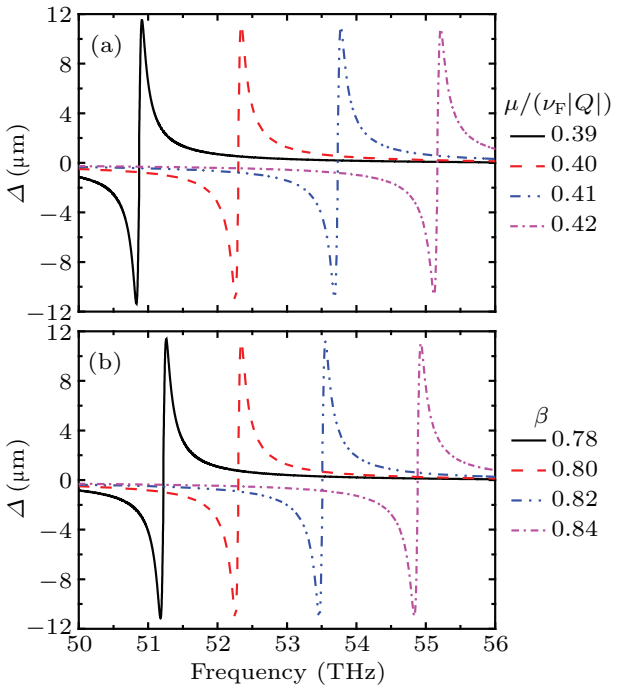


Fig. 4. The tunable-enhanced spatial IF shift. Panels (a) and (b) represent the spatial IF shift as a function of frequency at various Fermi energies and tilt degrees.

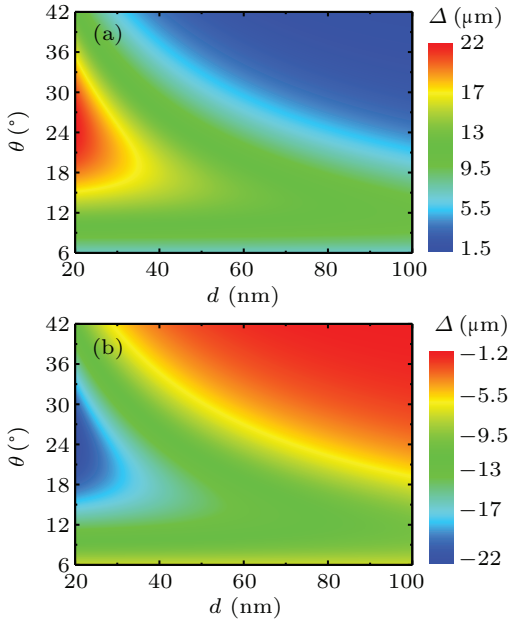


Fig. 5. Pseudo-color images of the spatial IF shift. Panels (a) and (b) denote the pseudo-color images of the spatial IF shift as functions of WSM thickness and incident angle at two frequencies of 52.34 THz and 52.26 THz, respectively.

Furthermore, the reflection coefficients exhibit the dependence of WSM thickness and incident angle. Therefore, the variation of WSM thickness and incident angle will lead to the change of the spatial IF shift. To illustrate the effects of WSM thickness and incident angle on the spatial IF shift, figures 5(a) and 5(b) denote the contours of the spatial IF shift as functions of WSM thickness and incident angle at two different frequencies. It is found that the large enhanced positive and negative spatial IF shifts can be realized. With the increase of WSM thickness, the incident angle should be declined to obtain the maximal enhanced positive and negative spatial IF shifts. Furthermore, the absolute value of the maximal enhanced spatial IF shift behaves as a decrease as the thickness of WSM increases, which is mainly caused by the declined value of $|r_{pp}|/|r_{ss}|$. In a word, the incident angle should be optimized to obtain the large enhanced spatial IF shift.

Finally, the amplitude of magnetic field induced by Weyl nodes can be represented equivalently with the Weyl node separation. Therefore, the Weyl node separation will affect the spatial IF shift significantly. The spatial IF shift at various Weyl node separations is shown in Fig. 6(a). It is found that the huge enhancement of the spatial IF shift can be realized at various Weyl node separations, and the relevant frequencies of maximal positive and negative spatial IF shifts maintain the same. However, as the Weyl node separation increases, the absolute enhanced spatial IF shift behaves as a large decrease. To further demonstrate the cause of the above phenomena, the value of $|r_{pp}|/|r_{ss}|$ as a function of frequency is shown in Fig. 6(b). Notably, large values of $|r_{pp}|/|r_{ss}|$ can be obtained at various Weyl node separations, while the value reduces as the Weyl node separation increases, which is consistent with the results of Fig. 6(a). Therefore, the larger enhanced spatial IF shift can be realized by decreasing the Weyl node separation.

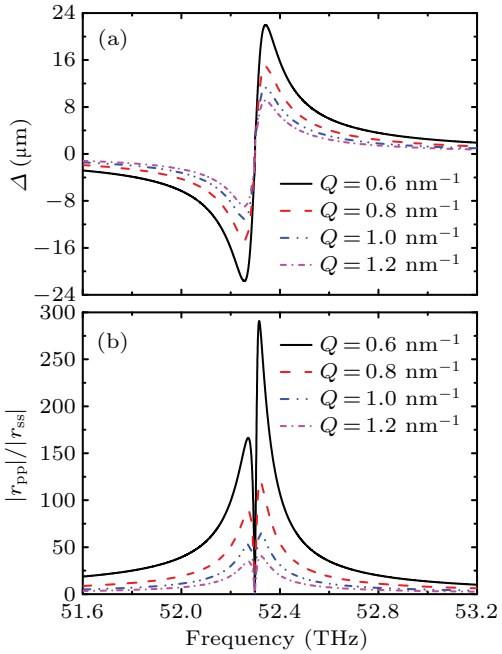


Fig. 6. The tunable-enhanced spatial IF shift with the Weyl node separation. Panels (a) and (b) represent the spatial IF shift and the value of $|r_{pp}|/|r_{ss}|$ as a function of frequency at various Weyl node separations, respectively.

4. Conclusions

In summary, the reflected spatial IF shift can be enhanced significantly based on the ENZ response induced different

sharp increasing trends of $|r_{pp}|$ and $|r_{ss}|$. What is more, the ENZ response can be adjusted by altering the tilt degree and Fermi energy, thus lead to the large enhanced spatial IF shift at different frequencies, and the tunable spatial IF shift varying from negative to positive with tilt degree enables the precise determination of WSM tilt degree. The enhanced spatial IF shift also shows the adjustability of WSM thickness and incident angle. By decreasing the Weyl node separation, the larger enhanced spatial IF shift can be obtained. Our findings supply easy and available methods to obtain the tunable enhanced reflected IF shifts of the TE-polarized wave with a WSM.

Acknowledgements

We would sincerely appreciate Drs. Jun Guo and Leyong Jiang for discussing the innovation of this paper with us. We would also thank to the doctoral candidate Jie Tang for his procedural help.

Project supported by the National Natural Science Foundation of China (Grant Nos. 61875133 and 11874269).

Data availability

The data that support the findings of this study are available within the paper.

References

[1] Bliokh K Y and Aiello A 2013 *J. Opt.* **15** 014001
[2] Bliokh K Y and Bliokh Y P 2006 *Phys. Rev. Lett.* **96** 073903
[3] Ling X H, Zhou X X, Huang K, Liu Y C, Qiu C W, Luo H L and Wen S C 2017 *Rep. Prog. Phys.* **80** 066401
[4] Hosten O and Kwiat P 2008 *Science* **319** 787
[5] Wang R S, Zhou J X, Zeng K M, Chen S Z, Ling X H, Shu W X, Luo H L and Wen S C 2020 *APL Photon.* **5** 016105
[6] Zhu W G, Xu H Q, Pan J T, Zhang S, Zheng H D, Zhong Y C, Yu J H and Chen Z 2020 *Opt. Express* **28** 25869
[7] Ling X H, Xiao W L, Chen S Z, Zhou X X, Luo H L and Zhou L 2021 *Phys. Rev. A* **103** 033515
[8] Ye G Z, Zhang W S, Wu W J, Chen S Z, Shu W X, Luo H L and Wen S C 2019 *Phys. Rev. A* **99** 023807
[9] Wu J P, Jiang L Y, Zeng R Z, Liang J J, Dai X Y and Xiang Y J 2022 *Phys. Rev. A* **105** 023508
[10] Tan X J and Zhu X S 2016 *Opt. Lett.* **41** 2478
[11] Xiang Y J, Jiang X, You Q, Guo J and Dai X Y 2017 *Photon. Res.* **5** 467
[12] Burkov A A and Balents L 2011 *Phys. Rev. Lett.* **107** 127205
[13] Ju L, Geng B S, Horng J, Girit C, Martin M, Hao Z, Bechtel H A, Liang X G, Zettl A, Shen Y R and Wang F 2011 *Nat. Nanotechnol.* **6** 630
[14] Hendry E, Hale P J, Moger J, Savchenko A K and Mikhailov S A 2010 *Phys. Rev. Lett.* **105** 097401
[15] Zyuzin A A and Burkov A A 2012 *Phys. Rev. B* **86** 115133
[16] Xu B, Qiu Z Y, Yang R, Dai Y M and Qiu X G 2019 *Acta Phys. Sin.* **68** 227804 (in Chinese)
[17] Hosur P, Parameswaran S A and Vishwanath A 2012 *Phys. Rev. Lett.* **108** 046602
[18] Ferreiros Y, Zyuzin A A and Bardarson J H 2017 *Phys. Rev. B* **96** 115202
[19] Wilczek F 1987 *Phys. Rev. Lett.* **58** 1799
[20] Wu L, Salehi M, Koirala N, Moon J, Oh S and Armitage N P 2016 *Science* **354** 1124
[21] Kargarian M, Randeria M and Trivedi N 2015 *Sci. Rep.* **5** 12683
[22] Wu J P, Zeng R Z, Liang J J, Jiang L Y and Xiang Y J 2021 *J. Appl. Phys.* **129** 153103
[23] Liu S Q, Song Y F, Wan T, Ke Y G and Luo Z M 2022 *Chin. Phys. B* **31** 074101
[24] Wu J P, Jiang L Y, Dai X Y and Xiang Y J 2022 *Phys. Rev. A* **105** 043519
[25] Wang G Q, Sun Z H, Si X Y and Jia S 2020 *Chin. Phys. B* **29** 077503
[26] Jia G Y, Huang Z X, Ma Q Y and Li G 2020 *Nanophotonics* **9** 715
[27] Liu S Q, Yang C F, Song Y F, Tang P, Ke Y G and Luo Z M 2021 *J. Phys. D: Appl. Phys.* **54** 285108
[28] Liberal I and Engheta N 2017 *Nat. Photonics* **11** 149
[29] Liu X G, Zang K, Kang J H, Park J, Harris J S, Kik P G and Brongersma M L 2018 *ACS Photonics* **5** 4484
[30] Edwards P P, Porch A, Jones M O, Morgan D V and Perks R M 2004 *Dalton Trans.* 2995
[31] Halterman K, Alidoust M and Zyuzin A 2018 *Phys. Rev. B* **98** 085109
[32] Halterman K and Alidoust M 2019 *Opt. Express* **27** 36164
[33] Chinotti M, Pal A, Ren W J, Petrovic C and Degiorgi L 2016 *Phys. Rev. B* **94** 245101
[34] Xu B, Dai Y M, Zhao L X, Wang K, Yang R, Zhang W, Liu J Y, Xiao H, Chen G F, Taylor A J, Yarotski D A, Prasankumar R P and Qiu X G 2016 *Phys. Rev. B* **93** 121110